Modal locking between vocal fold and vocal tract oscillations

A. Aalto[1], D. Aalto[2,3], J. Malinen[1], and M. Vainio[3]

[1] Dept. of Mathematics and Systems Analysis, Aalto University, Finland

[2] Dept. of Signal Processing and Acoustics, Aalto University, Finland

[3] Inst. of Behavioural Sciences (SigMe group), University of Helsinki, Finland

jarmo.malinen@aalto.fi

November 21, 2012

Abstract

The human vocal folds are known to interact with the vocal tract acoustics during voiced speech production; namely a nonlinear source-filter coupling has been observed both by using models and in *in vivo* phonation. These phenomena are approached from two directions in this article. We first present a computational dynamical model of the speech apparatus that contains an explicit filter-source feedback mechanism from the vocal tract acoustics back to the vocal folds oscillations. The model was used to simulate vocal pitch glides where the trajectory was forced to cross the lowest vocal tract resonance, i.e., the lowest formant F_1. Similar patterns produced by human participants were then studied. Both the simulations and the experimental results reveal an effect when the glides cross the first formant (as may happen in [i]). Conversely, this effect is not observed if there is no formant within the glide range (as is the case in [ɑ]). The experiments show smaller effect compared to the simulations, pointing to an active compensation mechanism.

Keywords. Speech modelling, vocal folds model, flow induced vibrations, modal locking.

PACS. Primary 4370Bk. Secondary 4370Gr, 4370Aj, 4370Mn.

1 Introduction

It is an underlying assumption in the linear source–filter theory of vowel production that the sound source (i.e., the vocal fold vibration) operates independently of the filter (i.e., the vocal tract, henceforth VT) whose resonances modulate the resulting vowel sound [1, 2]. This classical approach captures a wide range of phenomena in speech production, at least in male speakers. However, significant observations remain unexplained by the feedback free source-filter model, such as some fine structure in the phonation of a female singer near the lowest formant F_1. Instability of the fundamental (glottal) frequency f_0 has been detected acoustically [3] and at tissue level [4] when a singer performs an f_0-glide over F_1 on a steady vowel. As argued by Titze [5], the observed frequency jumps are due to a feedback coupling from the vocal sound pressure back to the glottal pulse generation, denoted there as the nonlinear source-filter coupling. Since F_1 usually lies well above f_0 in male phonation, this phenomenon occurs typically in female subjects when they are producing vowels with a low F_1. In laboratory experiments, Titze et al. found more instabilities in male subjects, possibly because males have less experience in suppressing unwanted instabilities [3].

The vocal source instabilities have been modeled by low-order mass-spring systems. A two-mass vocal folds model, coupled with a resonator tube, showed coupling related effects when the dimensions of the tube were manipulated [6]. Tokuda et al. simulated vocal pitch glides using a four-mass model to analyze the interactions between vocal register transitions and VT resonances [7].

For the current study, the f_0-F_1 cross-over phenomenon is approached from two complementary directions: 1) by simulating f_0-glides numerically on a steady vowel where F_1 is near f_0, using a dynamical vowel model that includes the filter-source feedback loop described above; and 2) by carrying out a related vowel glide production experiment on female test subjects.

2 The vocal folds model

2.1 Anatomy

Before introducing the glottis model, some anatomic details are reviewed, and physiological control mechanisms (actuated by muscles) affecting the speech characteristics are explained. Such explanation should be regarded as an idealization since the effect of a single muscle contraction can to some extent be compensated by other muscles involved. The glottis model is based

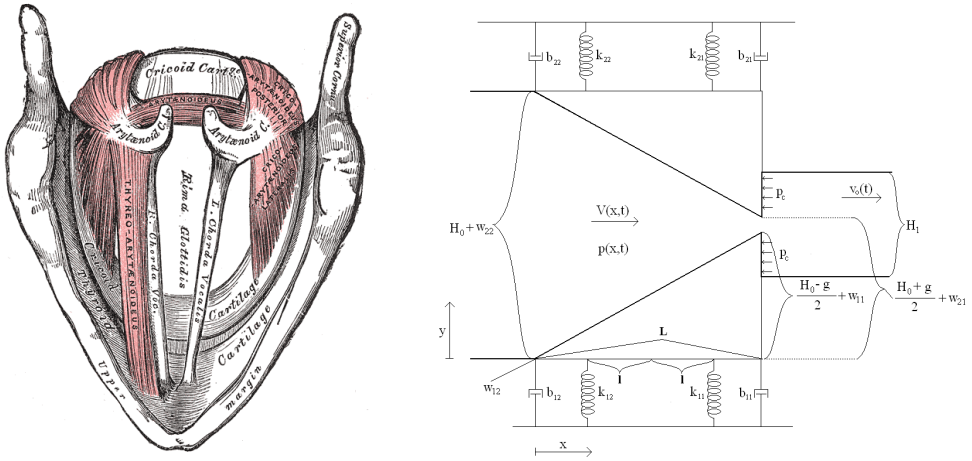

(a) (b)

Figure 1: (a): Sketch of the anatomy of the glottis according to Gray. (b): The geometry of the glottis model and the symbols used. The trachea (i.e. the channel leading from the lungs to glottis) is to the left in this sketch and the vocal tract is to the right.

on a further simplification of this idealization.

The vowel sound is produced by the self-sustained cut-off effect of the air flow from lungs, caused by a quasi-periodic closure of an aperture — known as the rima glottidis — by two string-like vocal folds. This process is called phonation, and the system comprising the vocal folds and the rima glottidis is known as the glottis. A single period of the sound pressure signal, produced by the glottal flow, is called the glottal pulse.

As shown in Fig. 1a, each vocal fold consists of a vocal cord (also known as a vocal ligament) together with a medial part of the thyroarytenoid muscle, and the vocalis muscle (not specified in Fig. 1a). Both vocal folds are attached to the thyroid cartilage from their anterior ends and to two corresponding arytenoid cartilages (i.e., the left and the right) from their posterior ends; see Fig. 1a. In addition to these three cartilages, there is the ring-formed cricoid cartilage whose location is inferior to the thyroid cartilage. The vocal folds and the associated muscles are supported by these cartilages as explained next.

Between each of the arytenoid cartilages and the cricoid cartilage, there are two muscles attached. These are the posterior and the lateral cricoarytenoid muscles, and they have opposite mechanical actions. Indeed, during phonation the vocal folds are adducted by the contraction of the lateral cricoarytenoid muscles, and conversely, abducted by the posterior cricoary-

tenoid muscles during, e.g., breathing. This control action is realized by a rotational movement of the arytenoid cartilages in a transversal plane. In addition, there is a fifth (unpaired) muscle — the arytenoid muscle — whose contraction brings the arytenoid cartilages closer to each other, thus reducing the opening of the glottis independently of the lateral cricoarytenoid muscles. These rather complicated control mechanisms regulate, in particular, the type of phonation in the breathy-pressed scale.

The fundamental frequency f_0 of a vowel sound is controlled by another mechanism that is actuated by two cricothyroid muscles (not visible in Fig. 1a). The contraction of these muscles leads to a rotation of the thyroid cartilage with respect to the cricoid cartilage. Because of this rotation, the thyroid cartilage inclines to the anterior direction, thus extending the vocal folds. The elongation of the string-like vocal folds leads to increased stress which raises the fundamental frequency of their longitudinal vibrations.

2.2 Glottis model

The anatomic configuration in Fig. 1a is modelled by a low-order mass-spring system shown in Fig. 1b, based on earlier work of Aalto [8, 10]. Numerical efficiency and theoretical tractability favor a low-order model, and the aim of the model is at functionality rather than at anatomic detail. The model is able to reproduce accurately the measured male glottal pulse obtained by inverse filtering [9, 11]. The model supports non-symmetric vocal fold vibrations, and both the fundamental frequency f_0 as well as the phonation type can be chosen by parameter values. Register shifts (e.g., from modal register to falsetto) are important phenomena not in the scope of this model. Accounting for register shifts would require either modelling the vocal folds as aerodynamically loaded strings or by a high-order mass-spring system that has a string-like "elastic" behavior.

The vocal fold model in Fig. 1b consists of two wedge-shaped vibrating elements that have two degrees of freedom each. The distributed mass of these elements can be reduced into three mass points which are located so that m_{j1} is at $x = L$, m_{j2} at $x = 0$, and m_{j3} at $x = L/2$. The elastic support of the vocal ligaments is approximated by two springs at points $x = aL$ and $x = bL$. The equations of motion for the vocal folds are given by

$$\begin{cases} M_1\ddot{W}_1(t) + B_1\dot{W}_1(t) + K_1W_1(t) = -F(t), \\ M_2\ddot{W}_2(t) + B_2\dot{W}_2(t) + K_2W_2(t) = F(t), \qquad t \in \mathbb{R}. \end{cases} \tag{1}$$

where $W_j = (w_{j1}, w_{j2})^T$ are the displacements of the right and left endpoints of the j^{th} fold, $j = 1, 2$. The respective mass, damping, and stiffness matrices

M_j, B_j, and K_j in (1) are

$$M_j = \begin{bmatrix} m_{j1} + \frac{m_{j3}}{4} & \frac{m_{j3}}{4} \\ \frac{m_{j3}}{4} & m_{j2} + \frac{m_{j3}}{4} \end{bmatrix}, \quad B_j = \begin{bmatrix} b_{j1} & 0 \\ 0 & b_{j2} \end{bmatrix}, \\ \text{and} \quad K_j = P \begin{bmatrix} a^2 k_{j1} + b^2 k_{j2} & ab(k_{j1} + k_{j2}) \\ ab(k_{j1} + k_{j2}) & b^2 k_{j1} + a^2 k_{j2} \end{bmatrix}. \tag{2}$$

The entries of these matrices are computed by means of Lagrangian mechanics. The damping matrices B_j are diagonal since the dampers are located at the endpoints of the vocal folds. The springs are located symmetrically around the midpoint $x = L/2$, so that $a = (L/2 + l)/L$ and $b = (L/2 - l)/L$. The control parameter $P > 0$ is used for simulating variable frequency f_0-glides for the purpose of this work.

During the glottal open phase (when $\Delta W_1(t) > 0$), the load terms of (1) are given by $F = (F_{A,1}, F_{A,2})^T$ as given in Eq. (6). During the glottal closed phase (when $\Delta W_1(t) < 0$), there are no aerodynamic forces apart from the acoustic counter pressure from the VT, denoted by p_c and properly introduced in the context of Eq. (7). Instead, there is a nonlinear spring force for the elastic collision of the vocal folds, given by the Hertz impact model [12]:

$$F = \begin{bmatrix} k_H |\Delta W_1|^{3/2} - \frac{H_0 - H_1/2}{2L} \frac{H_1}{2} h \cdot p_c \\ \frac{H_0 - H_1/2}{2L} \frac{H_1}{2} h \cdot p_c \end{bmatrix}. \tag{3}$$

The model geometry is shown in Fig. 1b, and it corresponds to the coronal section through the center of the vocal folds. As always in such biomechanical modelling [7, 12, 15], the lumped parameters of the mass-spring system are in some correspondence to the masses, material parameters, and geometric characteristics of the sound producing tissues. Such parameters are, e.g., the mass and stiffness matrices M_i and K_i, $i = 1, 2$, that appear in the equations of motion for the vocal folds (1).

More precisely, matrices M_i correspond to the vibrating masses of the vocal folds, including the vocal ligaments together with their covering mucous layers and (at least, partly) the supporting vocalis muscles. The elements of the matrices K_j are best understood as linear approximations of $k(s) = f/s$ where $f = f(s)$ is the contact force required for deflection s at the center of the string-like vocal ligament in Fig. 1a. It should be emphasized that the exact numerical correspondence of tissue parameters to lumped model parameters M_j and K_j is intractable (and for practical purposes, even irrelevant), and their values in computer simulations must be tuned using measurement data of f_0 and the measured form of the glottal pulse [9]. Even though the equations of motion are separate for both vocal folds, the parameters (hence,

the simulated vocal folds movements) are symmetric in all of the simulations reported in this paper.

3 Full model of vowel production

Having treated the modelling of the vocal folds, it remains to review the other components of the full model, i.e., the 1D incompressible flow model and the VT acoustics model.

These two subsystems are coupled so that the flow depends on the time-dependent glottal opening. Conversely, the flow produces aerodynamic forces on the vocal folds, and it also acts as the acoustic source to the resonating VT, modelled by Webster's equation. The acoustics of the sub-glottal air cavities is not modelled at all. The VT sound (counter) pressure gives rise to the filter-source feedback from VT to the glottal oscillations. Without this feedback, modal locking does not appear at all as can be verified by running model simulations with $f_0 \approx F_1$ with $p_c = 0$ in (6).

3.1 Flow

An incompressible 1D flow through the glottal opening with velocity v_o is described by

$$\dot{v}_o(t) = \frac{1}{C_{iner} h H_1} \left(p_{sub} - \frac{C_g}{\Delta W_1(t)^3} v_o(t) \right) \tag{4}$$

where the latter term inside the parentheses (representing the viscous pressure loss) is motivated by the Hagen–Poiseuille law in a narrow aperture. The constant sub-glottal pressure (subtracted by the ambient air pressure) is denoted by p_{sub}, and h is the width of the flow channel that is assumed rectangular. The parameter C_{iner} regulates the flow inertia, and C_g regulates the pressure loss in the glottis. Aalto et al. observed that C_{iner} effectively reveals the phonation type when other model parameters are estimated based on recorded speech signals [9].

The viscous pressure loss in (4) depends on the glottal opening at the narrowest point, i.e., ΔW_1. At the other end (i.e., towards the trachea) the opening is ΔW_2. These are given by (1) through

$$\begin{bmatrix} \Delta W_1 \\ \Delta W_2 \end{bmatrix} = W_2 - W_1 + \begin{bmatrix} g \\ H_0 \end{bmatrix}. \tag{5}$$

The parameter g is the glottal opening when there is no flow and the vocal folds do not vibrate ($W_1 = W_2 = 0$). In human anatomy, the parameter g is related to the position and orientation of the arytenoid cartilages.

In the glottis, the flow velocity $V(x,t)$ is assumed to satisfy the mass conservation law $H(x,t)V(x,t) = H_1 v_o(t)$ for incompressible flow where $H(x,t)$ is the height of the flow channel inside the glottis. In the model geometry of Fig. 1b, we have

$$H(x,t) = \Delta W_2(t) + \frac{x}{L}(\Delta W_1(t) - \Delta W_2(t)), \quad x \in [0,L].$$

Now the pressure $p(x,t)$ in the glottis is given by the two equations above and the Bernoulli law $p(x,t) + \frac{1}{2}\rho V(x,t)^2 = p_{sub}$ for static flow.

Since each vocal fold has two degrees of freedom, this pressure and the VT counter pressure p_c can be reduced to a force pair $(F_{A,1}, F_{A,2})^T$ where $F_{A,1}$ affects at the narrow (superior) end of the glottis ($x = L$) and $F_{A,2}$ at the wide (resp. inferior) end ($x = 0$). This reduction is carried out by using the total force and moment balance equations

$$F_{A,1} + F_{A,2} = h \int_0^L (p(x,t) - p_{sub})\, dx$$

and

$$L \cdot F_{A,1} = h \int_0^L x(p(x,t) - p_{sub})\, dx - p_c \cdot h \frac{H_1}{2} \frac{H_0 - H_1/2}{2}.$$

The moment is evaluated with respect to point $(x,y) = (0,0)$ for the lower fold and $(x,y) = (0,H_0)$ for the upper fold in Fig. 1b. Evaluation of these integrals yields

$$\begin{cases} F_{A,1} &= \frac{1}{2}\rho v_o^2 hL \left(-\frac{H_1^2}{\Delta W_1(\Delta W_2 - \Delta W_1)} + \frac{H_1^2}{(\Delta W_1 - \Delta W_2)^2} \ln\left(\frac{\Delta W_2}{\Delta W_1}\right)\right) - \frac{H_1(H_0 - H_1/2)}{4L} h p_c, \\ F_{A,2} &= \frac{1}{2}\rho v_o^2 hL \left(\frac{H_1^2}{\Delta W_2(\Delta W_2 - \Delta W_1)} - \frac{H_1^2}{(\Delta W_1 - \Delta W_2)^2} \ln\left(\frac{\Delta W_2}{\Delta W_1}\right)\right) + \frac{H_1(H_0 - H_1/2)}{4L} h p_c. \end{cases} \tag{6}$$

3.2 Vocal tract

The vocal tract acoustics is modeled by Webster's lossless horn resonator. The governing equation for the velocity potential $\Psi(s,t)$ is

$$\Psi_{tt}(s,t) - \frac{c^2}{A(s)} \frac{\partial}{\partial s}\left(A(s) \frac{\partial \Psi(s,t)}{\partial s} \right) = 0 \tag{7}$$

where c is the sound velocity. The parameter $s \in [0, L_{VT}]$ is the distance from the narrow (superior) end of the glottis measured along the VT center line, and L_{VT} is the length of the VT. The area function $A(\cdot)$ is the cross-sectional area of the VT, perpendicular to the VT center line. The sound pressure is given in terms of the velocity potential by $p = \rho \Psi_t$.

At the glottis end, the resonator is controlled by the flow velocity v_o from Eq. (4) through the boundary condition $\Psi_s(0,t) = -v_o(t)$. The resonator exerts a counter pressure $p_c(t) = \rho\Psi_t(0,t)$ to the vocal folds equations (1) through Eqs. (6), thereby forming a filter-source feedback loop. The boundary condition at lips is a frequency-independent acoustic resistance of the form $\Psi_t(L_{VT},t) + \theta c\Psi_s(L_{VT},t) = 0$ where θ is the normalized acoustic resistance [13].

3.3 Model parameters

The glottal flow equations (4) contain two independent parameters p_{sub}/C_g and C_{iner}; the mass-spring system contains three parameter matrices M_j, B_j, and K_j for $j = 1, 2$; and the resonator equations contain the area function $A(\cdot)$ in (7) and the acoustic termination parameter θ at the mouth.

Out of these parameters, p_{sub}/C_g and θ are determined from physical considerations and $A(\cdot)$ from anatomical data obtained by MRI. The area function used in simulations corresponds to [øː] as in Hannukainen et al [14]. The parameter range for C_{iner} has then been determined and validated so as to produce a realistic time-domain glottal pulse form [9]; the values corresponding to pressed phonation are used in this work. All these model parameter values introduced so far are equally valid for both female and male phonation.

It remains to consider the parameter matrices in the vocal folds equations (1) where the differences between female and male phonation are significant. Horáček et al. provide parameter values in male phonation [15, 12]. The parameter values (K_1, K_2) have been estimated indirectly by requiring the correct fundamental frequency f_0 [8]. The focus of this paper is in female phonation, and it is difficult to produce similar data for female subjects using literature. Thus, the typical nominal "male versions" of parameters M_j and K_j for $j = 1, 2$ (as given in Aalto [8, 9]) are scaled so as to obtain typical "female version" as explained above. This scaling is based on the data given by Titze [16].

Dimensional analysis and scaling yield

$$M_{\text{female}} = \lambda^{\alpha} M_{\text{male}} \qquad \text{and} \qquad K_{\text{female}} = \lambda^{\alpha-2} K_{\text{male}}$$

where the exponent $\alpha \in [2, 3]$ by physical grounds. Based on experimentation, the value used here is $\alpha = 2.3$. The scale factor $\lambda \approx 0.6$ is suggested by Titze [16] but here the value $\lambda = 0.55$ produces more female like phonation in simulations. The resulting increase in the resonances of (1) by factor $1/\lambda \approx 1.8$ reflects correctly the higher pitch of the female voice.

The f_0-glide is simulated by additional scaling of the matrices K_j whereas the matrices M_j are kept constant. This is based on the assumption that the vibrating mass of vocal folds is not significantly reduced when the speaker's pitch increases; a reasonable assumption as far as register changes are excluded. The authors would like to remark that the relative magnitudes of M_j and K_j essentially determine the resonance frequencies of model (1). However, attention must be paid to their absolute magnitudes using, e.g., dimensional analysis since otherwise the load terms $\pm F(t)$ in (1) (containing the aerodynamic forces, contact force between the vocal folds during the glottal closed phase, and the counter pressure from the VT) would scale in an unrealistic manner.

The damping parameters $b_{ji},\ i,j = 1,2$, in Eq. (2) play an important but problematic role in glottis models. If there is too much damping (while keeping all other model parameters fixed), sustained oscillations do not occur. Conversely, too low damping will cause instability in simulated vocal folds oscillations. The magnitude of physically realistic damping in vibrating tissues is not available, and the present model could possibly fail to give a quasi-stationary glottis signal even if realistic experimental damping values were available for use. For simplicity, we set $b_{ji} = \beta > 0$ for $i,j = 1,2$, and the value of glottis loss β is adjusted separately for each parameter value set in order to obtain stable but sustained oscillation. In particular, parameter β is adjusted every 100 ms during the f_0-glide simulations presented below. The damping remains always so small that its lowering effect on the resonances of the mass-spring system (1) is negligible.

Let us conclude by discussing the parameter magnitudes in Eq. (1). The total vibrating mass is $m_{j1}+m_{j2}+m_{j3} = 0.48\ g$ for male and $0.12\ g$ for female phonation. The total spring coefficients are $k_{j1} + k_{j2} = 193\ N/m$ for male and 161.3 N/m for female phonation using the nominal values, i.e., when $P = 1$ in Eq. (2). The nominal values yield $f_0 = 110$ Hz for male and 187 Hz for female phonation. If the characteristic thickness of the vocal folds is assumed to be about 5 mm, these parameters yield a magnitude estimate for the elastic modulus of the vocal folds by $E \approx \frac{k_{j1}+k_{j2}}{Lh} \cdot 5 \cdot 10^{-3}\ m \approx 6.6\ kPa$. This is in good comparison with Fig. 7 in Chhetri et al.[17] where estimates are given for the elastic modulus of *ex vivo* male vocal folds between 2.0 kPa and 7.5 kPa for different parts of the vocal folds.

3.4 Numerical realization

The model equations are solved numerically using MATLAB software and custom-made code. The vocal fold equations of motion (1) are solved by the fourth order Runge–Kutta time discretization scheme. The discontinuity of

the load $F(t)$ at $\Delta W_1(t) = 0$ is dealt with by an interpolation procedure detailed in Aalto (Section 2.4)[8]. The flow equation (4) is solved by the backward Euler method. The VT is discretized by the FEM using piecewise linear elements ($N = 100$) and the physical energy norm of Webster's equation. Crank–Nicolson time discretization is used, and the time step is always 20 μs.

4 Simulation results

Frequency glides of vowel [ø:] are simulated near the lowest formant F_1 or its subharmonic $F_1/2$. In these simulations, F_1 (determined from spectrograms of simulated vowel signals) coincides with the lowest resonance of the VT (solved independently from the eigenvalue problem associated to (7) and the boundary conditions). To produce the glides, parameter P in Eq. (2) is increased (or decreased) as a quadratic function of time. Then the oscillation frequency of the vocal fold model (1) in the absence of the counter pressure p_c — denoted by $\tilde{f}_0$ — increases (respectively, decreases) as a linear function of time. This can be observed in simulation results if the filter-source feedback mechanism is disconnected by setting the counter pressure $p_c = 0$ in Eq. (6). When using $p_c(t) = \rho\Psi_t(0, t)$ with Eq. (7), the observed fundamental frequency f_0 of the whole system does not behave linearly in time (in contrast to $\tilde{f}_0$) but exhibits jumps near F_1 (and $F_1/2$) as shown in Fig. 3b. This behavior, the modal locking, is due to the filter-source feedback [5, 4].

Changing the area function $A(\cdot)$ in Eq. (7) to correspond some other vowel than [ø:] does not change the results of model simulations apart from formant, and hence, modal locking frequencies.

4.1 f_0–F_1 crossover

Frequency f_0-glides of length 2 s are simulated by varying the parameter P of the glottis model so that 350 Hz $< \tilde{f}_0 <$ 810 Hz linearly in time. The increasing phase is shown in the spectrogram Fig. 3a with an auxiliary line showing the glide of $\tilde{f}_0$ and another line showing $F_1 = 647$ Hz. It is observed that f_0 coincides first with $\tilde{f}_0$, but then it suddenly jumps upwards to F_1 when it reaches about 470 Hz. The wave form of the glottal pulse near the transition is a superposition of two signals with frequencies $\tilde{f}_0$ and F_1. When $\tilde{f}_0$ exceeds F_1, then f_0 and $\tilde{f}_0$ coincide again. The qualitative behavior is sketched in the rising part of Fig. 3b.

In a downwards glide the behavior is almost symmetric. First $f_0 = \tilde{f}_0$ descends down to F_1 where f_0 locks for a while. The latent glottal model

frequency $\tilde{f}_0$, of course, goes down linearly without change. After a time lag, f_0 is released from F_1 and drops suddenly to $\tilde{f}_0$. This behavior is shown in the descending part of Fig. 3b.

As can be seen in Fig. 3b, there are two periods (of length $T_u, T_d > 0$) during which $f_0 = F_1$. Let us denote the corresponding frequency jumps by $\phi_u, \phi_d > 0$. By Fig. 3b we see $\phi_u/T_u = \phi_d/T_d$ is determined by the ascend and descend rate of the simulated, symmetric $\tilde{f}_0$-glide. We observe $\phi_d > \phi_u$ consistently in all simulations, and if the $\tilde{f}_0$-glide is very slow, we observe that $\phi_d \approx \phi_u$ and Fig. 3b becomes symmetric. Simulating extremely slow glides (during which the parameter P can be regarded as a constant), it is observed that the jumps ϕ_d and ϕ_u have a common lower bound $\phi \approx 174$ Hz. This number can be regarded as the "true" magnitude of the simulated frequency jump, and it is in reasonable correspondence with the results reported in [3, 5].

It was noted above that $\phi_d > \phi_u$. One way to understand this asymmetry is in terms of the energy dissipation from VT resonance modes. The only energy losses in Eq. (7) are due to the dissipative boundary condition at lips. During a downwards glide, there is a locking of f_0 at F_1, and then a lot of energy is contained in the corresponding eigenmode of the joint system, comprising the VT air column and the vocal fold masses. For the vocal folds oscillations to get "unlocked" from this eigenmode, most of this energy must first be dissipated either by mouth radiation or by dispersion to other eigenmodes as a consequence of nonlinearity and lack of time invariance of the model. The dissipation rate may be slow compared to the speed of decrease of the $\tilde{f}_0$-glide. Thus, the latent frequency $\tilde{f}_0$ may have fallen far below F_1 before unlocking of f_0 may take place. It is therefore expected that the time delay T_d is sensitive to relative magnitudes of losses and amounts of energy stored in vocal folds and VT, and this is supported by the simulations. Indeed, T_d becomes very large if the vocal folds oscillation amplitude is small during the glide.

4.2 Glides near subharmonics of F_1

Similar f_0-glides are produced as explained above but now 187 Hz $< \tilde{f}_0 <$ 390 Hz linearly during 2 s time interval. The subharmonic $F_1/2 = 324$ Hz lies in this interval, and two kinds of behavior are observed. First, f_0 increases from below in Fig. 2a until $F_1/2$ is reached; there is no locking at $F_1/2$ but f_0 jumps one octave up and locks at F_1. Second, the phenomenon does not appear at all if the vocal fold oscillation amplitude is large enough.

In Fig. 2b there is a downward glide near $F_1/2$. First and third harmonics of f_0 have a static part matching F_1 and $2F_1$ respectively. It may be possible

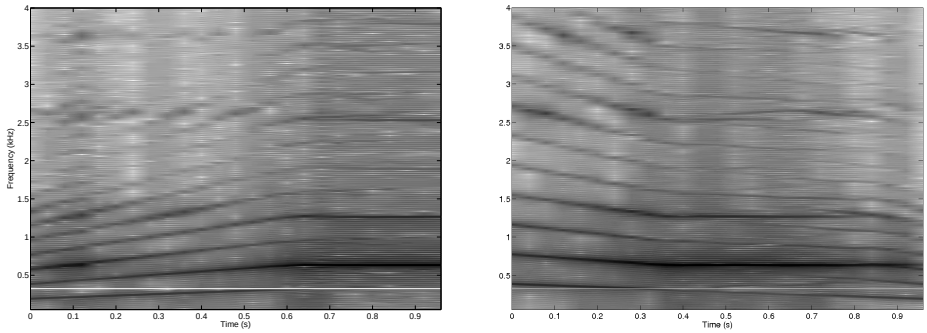

Figure 2: (a): Upwards f_0-glide over $F_1/2$. (b): Downwards f_0-glide over $F_1/2$.

that f_0 is "partly locked" to $F_1/2$ but there is a clear component that develops with $\tilde{f}_0$. Such a complicated spectral behavior emphasizes the surprising dynamical richness of the vowel production model presented in this paper.

5 Glide production experiment

The simulation results and earlier experimental evidence [3] suggest that consequences of filter-source feedback should be detectable at crossings of frequencies f_0 and F_1. Unfortunately, determining the precise crossing time of f_0 and F_1 in vowel glides is difficult when based on the acoustic signal alone. Indeed, the harmonics $2f_0, 3f_0, \ldots$ do not coincide with the bandwidth of F_1 if $f_0 \approx F_1$. If f_0 follows successfully a slowly varying reference glide (as should happen in these experiments), it is then far from a persistently exciting signal that would be required for precise detection of F_1. In a similar glide production experiment, Titze et al. [3] asked the test subjects to produce a spectrally rich vocal fry adjacent to every glide. A good estimate for F_1 can be obtained this way, but the formant may creep during the glide. The subject is, in fact, expected to use various techniques to avoid modal locking in order to produce audibly clean vowel glides, and F_1 position is expected to be affected near f_0. We conclude that obtaining the crossing time of f_0 and F_1 from acoustic signals remains a difficult estimation problem.

Rather than replicating the experimental arrangements of Titze et al. [3], a complementary approach is taken here without F_1 as a controlled variable. This is achieved by eliciting vocal glides for two different vowels [ɑ] and [i], where [i] has F_1 within the f_0 glide range, and F_1 of [ɑ] is as far as possible from the same range. The model simulations predict that the f_0-trajectories corresponding to [ɑ] and [i] should have distinctly different characteristics

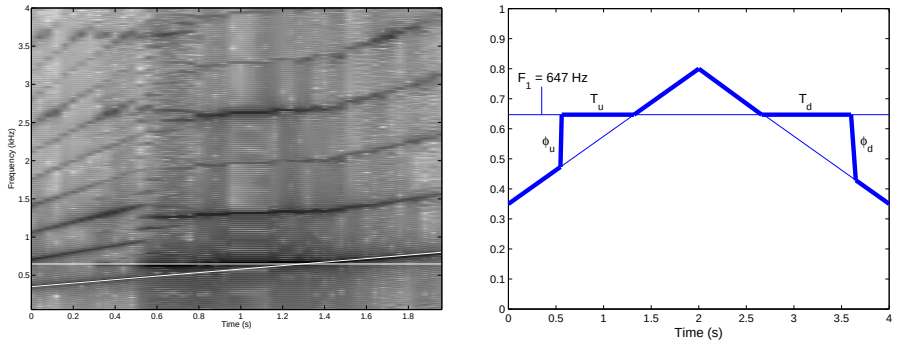

Figure 3: (a): f_0-glide 350 Hz – 810 Hz. (b): A sketch of the modal locking in an f_0-glide over F_1 first upwards and then downwards. The thick (thin) line shows f_0 (resp. $\tilde{f}_0$) during the glide.

that should be detectable in natural glide productions.

5.1 Quantification of the jumping pattern

During a modal locking episode, f_0 is expected to jump as in Fig. 3. To quantify the jump effect for statistical analysis, the Duration Ratio (DR) of the glide $f_0 = f_0(t)$ is defined. For frequencies $f_A < f_a < f_b < f_B$, DR is defined by

$$DR(f_0) = \frac{t_b - t_a}{t_B - t_A} \tag{8}$$

where (t_A, t_B) is the longest open interval where $f_A \leq f_0(t) \leq f_B$ for all $t \in (t_A, t_B)$, and (t_a, t_b) is the longest open interval where $f_a \leq f_0(t) \leq f_b$ for all $t \in (t_a, t_b)$ such that $[t_a, t_b] \subset (t_A, t_B)$, i.e., $t_A < t_a \leq t_b < t_B$. This implies $0 \leq DR(f_0) \leq 1$ for any glide f_0. By definition, DR does not depend on the direction or the speed of the glide in the sense that $DR(f_0) = DR(\tilde{f}_0) = DR(f_0^a)$ where $\tilde{f}_0(t) = f_0(-t)$ and $f_0^a(t) = f_0(at)$ for $a > 0$.

In the current experiments, all octave glides are between 200 Hz and 400 Hz, and the parameter values for Eq. (8) are always $f_A = \gamma \cdot 200$ Hz ≈ 230 Hz, $f_a = \gamma f_A \approx 264$ Hz, $f_b = \gamma f_a \approx 303$ Hz, and $f_B = \gamma f_b \approx 348$ Hz where $\gamma = 2^{1/5} \approx 1.148698$. Hence, the octave $[200\,\text{Hz}, 400\,\text{Hz}]$ is divided into five intervals equal in logarithmic scale. We say that the glide f_0 is full if its range contains all of the interval $[f_A, f_B]$. If $f_0(t) = a2^{kt}$ for some $a > 0$, $k \neq 0$, and $t \in [0, T]$ is a full glide, then we call it logarithmically linear and we have $DR(f_0) = 1/3$ which can be regarded as the nominal value of DR on full glides in the absence of any perturbations.

For an ideal logarithmically linear full glide f_0 with a single modal locking

"jump" as in Fig. 3, we have $DR(f_0) < 1/3$ if the jump intersects f_b but not f_a or f_B. Similarly, $DR(f_0) > 1/3$ if the jump intersects f_a but not f_b or f_A. The jump size and the jump position $\tilde{F}$ (satisfying $\tilde{F} = F_1$ in glide simulations) change the DR in a practically convenient way: to see this, a numerical experiment was performed. Full, logarithmically linear jump patterns were constructed using jump size of 100 Hz and one million tokens of $\tilde{F}$ drawn from a normal distribution with $\mu = 300$ Hz and $\sigma = 50$ Hz. This produced $\mathbb{E}[DR] = 0.308$ and $SD[DR] = 0.325$. Keeping σ constant but varying μ gave the following values: $\mathbb{E}[DR] = 0.354$ and $SD[DR] = 0.270$ at $\mu = 250$ Hz; $\mathbb{E}[DR] = 0.240$ and $SD[DR] = 0.270$ at $\mu = 350$ Hz; and finally $\mathbb{E}[DR] = 0.333$ and $SD[DR] = 0.002$ at $\mu = 600$ Hz as expected.

The experiment is designed so as to create situations where glides of [i] are more likely to have lower DR compared to glides of [ɑ], due to modal locking induced f_0-jumps over f_b for [i] but not at all for [ɑ]. More precisely, the position of F_1 of [i] is expected to be roughly at 300 Hz (which, of course, explains the choice of f_b above), and the position of F_1 of [ɑ] is likely to be above 600 Hz. Thus, simulated model predictions of jump patterns can be formulated as the statistically testable hypotheses:

Hypothesis 1. *The population mean of the Duration Ratio on full [i]-glides* $f_0^{[i]}$ *and on full [ɑ]-glides* $f_0^{[\alpha]}$ *satisfies* $\mathbb{E}\left[DR(f_0^{[i]})\right] < \mathbb{E}\left[DR(f_0^{[\alpha]})\right]$.

Hypothesis 2. *The population mean of the Duration Ratio on full [i]-glides* $f_0^{[i]}$ *satisfies* $\mathbb{E}\left[DR(f_0^{[i]})\right] < 1/3$*, and the population mean of the Duration Ratio on full [ɑ]-glides* $f_0^{[\alpha]}$ *satisfies* $\mathbb{E}\left[DR(f_0^{[\alpha]})\right] = 1/3$.

5.2 Subjects and the recording arrangement

Eleven native Finnish speaking female students at the University of Helsinki were recruited for the experiment. Females were chosen as subjects because (non-singing) males have typically little familiarity of using their vocal range around their naturally occurring F_1. Hence, using males would probably lead to an overly high rejection rate of glide samples and excursions to falsetto register in otherwise successful glides.

None of the participants reported any hearing or voice problems, and they had not received professional training in singing although some of them had a musical hobby (like violin playing). The participants were informed of the general purpose of the research and presented with the gliding task. There was a short familiarization period before the actual experiment during which the participants could practice the gliding with the vowel [ɑ]. Some

participants were helped to find the right pitch range. The data was recorded in a sound-proof studio with a high-quality microphone (AKG C4000B), and digitized with Digidesign (DIGI 002) and ProTools v.9.

5.3 Glide imitation stimuli

The subjects were instructed to produce frequency glides by following a spectrally neutral, synthesized reference glides from 200 Hz to 400 Hz. Every reference glide started and ended with a constant frequency part of 0.25 s to create a sensation of the right initial (resp., final) pitch of the glide. The instruction was given as a pre-recorded 0.5 s sample of either of the vowels, followed by three beeps (countdown beep: 0.25 s signal followed by 0.75 s silence). The beeps had the pitch of the onset value of the desired glide (either 200 Hz or 400 Hz). The glides and beeps were frequency modulated triangle waves; the triangle wave function $s(t)$ is a 2π-periodic function with constant slope (except for multiplicities of 2π). The upward glides are given by $s(2\pi\omega(t))$ with $\omega(t) = \frac{T \cdot 200\text{Hz}}{\log 2}(2^{t/T} - 1)$ for $t \in [0, T]$ where T is the duration of the glide (either 1.5 s or 3.0 s). The instantaneous frequency of such a glide is given by $\frac{\partial\omega(t)}{\partial t} = 2^{t/T} \cdot 200\text{Hz}$ which was assumed to be equal with the perceived pitch.

5.4 Experimental setup

The subjects were asked to imitate the pitch of reference glides by producing them with a prolonged, spoken [ɑ] or [i]. The subjects heard the reference glide from earphones at a volume that was adjusted for each subject to be as loud as possible without being unpleasant. The purpose of this arrangement was to hinder the subjects from hearing their own production easily and to elicit good phonation.

The data was gathered following a factorial 2^3 design with direction (either fall or rise), duration (either fast 1.5 s or slow 3 s), and vowel (either [ɑ] or [i]) as factors. Each subject had her own pseudo-randomized list of stimuli. The lists were constructed so that the different stimulus types would be randomly and evenly distributed in the trial: the stimuli were divided in blocks of 24 where each stimulus condition occurred three times, three identical stimuli were never in a row (not even over the blocks), four identical glide directions, vowels, or glide speeds were never in a row.

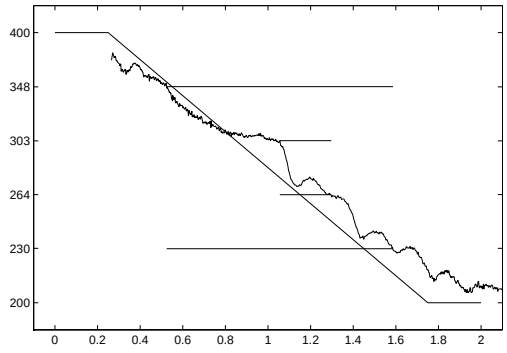

Figure 4: A typical production of a vowel glide [i]. The linear line depicts the guiding signal and the zig-zagging line shows the fundamental frequency of the glide. The intervals corresponding to the mid-frequency and total durations are shown as horizontal lines.

5.5 Data analysis

Three subjects were disqualified since they did not learn the gliding pattern well enough. Most of their productions had at least one of the following characteristics: the glide was one octave away from the guiding glide signal, the glide pattern was missing (static or undulating pitch), or the range of the glide was limited to less than a quarter. The remaining eight subjects had no difficulties in the gliding task.

A total of 864 glides were processed further. The vocal pitch was extracted by cross-correlation using Praat (Praat 5.2.21; default parameters with admissible range from 200 Hz to 400 Hz). The pitch trajectories of the glides were automatically chopped from the audio signal, based on the timing of the guiding signals and further analyzed in MATLAB. A custom-made algorithm was used to calculate $DR(\cdot)$ from the data.

The glides were analyzed for their "fullness" to exclude the related bias in Duration Ratio values. The range from f_A to f_B was divided in ten equally long frequency bands in logarithmic scale. If some of the bands did not contain a value of f_0, the glide was not considered full. This led to exclusion of 8 glides (1%). A mixed linear model was fitted to the remaining data using statistical software package R (version 2.14.0) and the model parameter selection was based on log-likelihoods [18]. Both of the Hypotheses 1 and 2 were independently tested by t-tests.

A typical production is shown in Fig. 4 where the f_0 trajectory of a fast falling [i] is given. The reference glide is the diagonal line with flat ends at $t = 0, 2$. The four horizontal lines indicate the critical frequencies

f_A, f_a, f_b and f_B as introduced above. The corresponding time intervals for Eq. (8) are given by $(t_A, t_B) = (0.52, 1.59)$ and $[t_a, t_b] = (0.77, 1.03)$, yielding $DR(f_0) = 0.243 < 1/3$.

5.6 Results

The estimated means and standard deviations for DR at each eight factor combination groups are shown in the Table 1. The estimated mean DR's of [ɑ] are consistently larger than those of [i] (see Hypothesis 1), and also the nominal DR value $1/3 = 0.33\ldots$ is above the estimated mean of DR for all four [i] conditions.

Table 1: *The means and standard deviations for the Duration Ratio (DR) over each factor combination.*

Condition	Mean	SD	N
Fast fall [ɑ]	0.341	0.099	106
Fast fall [i]	0.324	0.108	105
Fast rise [ɑ]	0.331	0.084	108
Fast rise [i]	0.312	0.073	108
Slow fall [ɑ]	0.337	0.106	107
Slow fall [i]	0.326	0.104	106
Slow rise [ɑ]	0.340	0.102	108
Slow rise [i]	0.320	0.105	108

Considering the four vowel pair samples separately, Hypothesis 1 on the population mean DR holds at $p \leq 0.05$ by fast rises only (Welch two sample (one-sided) t-test with $df = 209$, $t = -1.8$, $p = 0.04$). The estimated mean and standard deviation of DR using all [i] glides are 0.320 and 0.098 ($n = 427$), respectively. For all [ɑ] glides, the respective values are 0.337 and 0.098 ($n = 429$). Hence, Hypothesis 1 is verified using the full data set (Welch two sample test with $df = 853$, $t = -2.5$, $p < 0.01$).

The first part of Hypothesis 2 is verified at $p = 0.05$ by fast rise [i] (one-sided t-test, $df = 107$, $t = -3.1$, $p = 0.001$) and also by using all [i] glides as the sample (one-sided t-test with $df = 426$, $t = -2.7$, $p < 0.01$). The population mean of DR over all [ɑ] is not significantly different from the nominal value ($df = 428$, $|t| < 0.9$, $p < 0.4$) but the probability of a Type II Error is still large. Thus, the latter part of Hypothesis 2 is not supported statistically conclusively by the current dataset.

A mixed effects model supports the previous observations. Glide $j = 1, \ldots, n_i$ from subject i produces the DR value denoted by $y_{i,j}$, given by the

Table 2: *The linear mixed-effects model results for Duration Ratio (DR). The fixed factors are vowel, direction and speed; the subjects are treated as random factors.*

Factor	Estimate	Std. Error	t-value	p-value
Intercept	0.338	0.009	39.0	0
Vowel ([i])	-0.017	0.007	-2.5	0.01
Direction (rise)	-0.007	0.007	-0.98	0.3
Speed (slow)	0.004	0.007	0.56	0.6

mixed effects model

$$y_{i,j} = \beta_0 + d_{i,j}\beta_1 + s_{i,j}\beta_2 + v_{i,j}\beta_3 + b_i + e_{i,j}$$

where the fixed factors (with numerical levels 0 or 1) are the glide direction $d_{i,j}$, the glide speed $s_{i,j}$, and the vowel type $v_{i,j}$. The test subject related random factors $b_i \sim N(\mu_i, \sigma_i)$ are independent from the experimental errors $e_{i,j} \sim N(0, \sigma)$. As can be seen in the Table 2, the vowel type has a significant effect (ANOVA, $df = 845$, $|t| > 2.5$, $p = 0.011$) while the effect of the direction and speed are not significant ($df = 845$, $|t| < 1$). In a more complicated model taking into account all the interactions of the factors, the log-likelihoods of the models were lower, and the interactions were never significant.

6 Discussion

As is usual in model validation experiments, the measurement data is much more ambiguous than the results of numerical simulations. The reconciliation of simulated and measured data is difficult because of the following two main challenges:

1. The computational model could give an unrealistically strong indication of modal locking because of unmodelled physics (such as subglottal acoustics, supraglottal turbulence, and energy losses).

2. The humans have active control mechanisms (without counterparts in the computational model) that are expected to reduce the observable effects of modal locking.

Subglottal acoustics has been completely excluded from the computational model. The main reason for this is the lack of experimental data that would

be required to reproduce the extremely difficult absorbing boundary condition that the progressively subdividing system of bronchi and the alveoles constitute. Moreover, in the four-mass glottis model of Tokuda et al. [7], subglottal acoustics play a minor role compared to the supraglottal acoustics. Hence, the coupling of the subglottal acoustics and the vocal fold oscillations does not seem to be the primary source of the discrepancy between simulations and experimental results.

The supraglottal aerodynamics might have influence on the vowel glides. State-of-the-art Computational Fluid Dynamics (CFD) models indicate significant vorticity above the glottis [19]. The vorticity-induced aerodynamic force to the vocal folds is a genuinely fluid mechanical feature that is beyond the scope of the acoustic theory of speech as well as simple Bernoulli flow models in VT. Evaluating the contribution of this force would also require a more refined CFD model than is usually available.

In low frequency glide productions, the larynx moves vertically [20]. However, the simulated vowel glides were produced using a fixed area function, and no movement in the larynx area is taken into account at all. The increased pitch is a consequence of the elongation and higher stress in vocal folds due to rotation of the thyroid cartilage in the anterior direction. Towards the end of a glide production, larynx moves as a consequence of both the contracting thorax and the control actions required for variable pitch. These two mechanisms either oppose or reinforce each other depending on the direction of the glide. All this applies equally to VT geometries of [ɑ] and [i].

Considering the latter challenge 2 above, the direct modeling of the auditory, motor, and muscular mechanisms behind the task performance seems unfeasible at the moment. Fortunately, the experiments can be arranged in a manner that downplays or even interferes with the active control mechanisms. For this reason, trained singers are – somewhat paradoxically – excluded as test subjects even though producing vowel glides resembles very much a singing exercise. (Recall that non-singing males were excluded for the opposite reason.) The drawback of having non-singers was that some of the subjects could not perform the glide task satisfactorily which may have led to selection bias. However, these subjects are expected to be less familiar in their vocal pitch control which would lead to less accurate compensation (and hence, better detection in experiments) of the modal locking disturbance.

Control mechanisms based on auditory feedback have been shown to rapidly and accurately compensate deviations from target glides in glide production [21]. This could lead to asymmetric f_0 trajectories in terms of the glide direction because of different delays in control and observation. Recalling the simulated f_0 trajectory in Fig. 3b, such a modal locking event during

a rising glide is detectable only right after a large jump has already occurred while a modal-locking event during a fall can, in principle, be detected when the f_0 has just ceased to decline. Considering the control delay alone, suppose that the compensation strategy against modal locking were only based on the auditory observation with an identical delay (of say 80 ms) for both rising and falling glides. Then the fall would be less perturbed by the modal locking event because then the control action has more time to react. For obvious reasons, however, the auditive observation of modal locking events in falling glides could be more delayed compared to rising glides for f_0 trajectory profiles as in Fig. 3b. All in all, there are convincing reasons why rising and falling glides in experiments are not expected to be symmetric, and such asymmetry could explain the fact that the fast rising [i] stands out when verifying Hypothesis 2 above. It must be noted that the fast rising [i] does not similarly stand out using the mixed effects model.

Not much can be concluded from the observed numerical values of DR on the two vowel classes. First, the distribution of F_1 for [i] glides was not controlled while it is known by the numerical experiment that a relatively small variation of 50 Hz in $\tilde{F}$ affects the mean values of DR. Second, DR is a nonlinear functional, and one has to be careful in interpretations by continuity; e.g., DR may have very large or very small values for large jumps that cross both f_A and f_B. Third, the jumps never occur instantaneously in the data but rather show an accelerated pitch movement giving DR values closer to 1/3 than in the simulations. Fourth, the dynamics of the pitch following exercise is not understood in such detail that its effect on DR could be evaluated at all. Such dynamics may be a source of systematic error in the estimated DR values, resulting in the lack of verification of the latter part of Hypothesis 2 concerning [ɑ] glides.

The computational model predicts modal locking to subharmonics of the vowel formants as well. These are characterized by jumps of one octave, and, if they took place, they would have gone unnoticed in the data processing. Indeed, the pitch detection algorithm admitted only results inside one octave [200 Hz, 400 Hz] which was the nominal gliding range. Otherwise, large jumps were not observed for [ɑ] in the current dataset but such jumps have been observed in other experiments [4].

7 Conclusions

Results from numerical simulations and experiments have been reported on vowel glides. The simulations show a robust and large effect of modal locking of f_0 to F_1 whenever the frequencies coincide. The experimental data

shows a reduced effect of the same kind, supporting the computational model. Hence, experimental results give positive evidence for the existence of significant filter-source feedback in human glide productions even in an experimental setting where the frequency jumps were implicitly asked to be avoided. Moreover, the results suggest that compensatory mechanisms are employed to avoid filter-source feedback induced f_0 jumps near the formant frequency F_1.

Uncontrolled f_0 jumps occur frequently in the phonation of boys during the puberty [22]. Changes in the vocal folds and the growing larynx make it difficult for them to produce natural intonation contours or to sing musical melodies. These observations may be partly due to modal locking since the relevant compensatory mechanisms are expected to require re-tuning after a radical change in the geometric dimensions of both the VT and the vocal folds. If the poorly compensated filter-source interaction were a significant cause, then these f_0 jumps would have to be more frequent in VT configurations where F_1 is low; i.e., in high vowels such as [i] and [u].

Finally, we remark that the active compensation mechanisms to counteract the filter-source feedback could perhaps be observed directly. It is expected that especially trained singers would adjust their VT in order to keep the formant and the vocal pitch apart from each other.

Acknowledgements

The authors were supported by the Finnish graduate school in engineering mechanics, Finnish Academy grant Lastu 135005, the Finnish Academy projects 128204 and 125940, European Union grant Simple4All (grant no. 287678), Aalto Starting Grant, and Åbo Akademi Institute of Mathematics. The authors would like to thank O. Engwall for the area function used in the simulations.

References

[1] Chiba, T. and Kajiyama, M. *The Vowel, its Nature and Structure*. Tokyo-Kaiseikan Publishing Company Ltd., 1941.

[2] Fant, G. *The Acoustic Theory of Speech Production*. Moulton, The Hague, 1960.

[3] Titze, I., Riede, T., and Popolo, P. Nonlinear source-filter coupling in phonation: Vocal exercises, *J. Acoust. Soc. Am.*, 123(4):1902–1915,2008.

[4] Zañartu, M., Mehta, D. D., Ho, J. C., Wodicka, G. R., and Hillman, R. E. Observation and anlysis of *in vivo* vocal fold tissue instabilities produced by nonlinear source-filter coupling: A case study. *J. Acoust. Soc. Am.* 129:1, 326–339, 2011.

[5] Titze, I. Nonlinear source-filter coupling in phonation: Theory, *J. Acoust. Soc. Am.*, 123(5):2733–2749,2008.

[6] Hatzikirou H., Fitch W. T., and Herzel H. Voice Instabilities due to Source-Tract Interactions, *Acta Acustica united with Acustica*, 92:468–475, 2006.

[7] Tokuda, I. T., Zemke, M., Kob, M., and Herzel, H. Biomechanical modeling of register transitions and the role of vocal tract resonators. *J. Acoust. Soc. Am.* 127:3, 1528–1536, 2010.

[8] Aalto, A. *A low-order glottis model with nonturbulent flow and mechanically coupled acoustic load*, Master's thesis, TKK, Helsinki, 2009. Available at `http://math.aalto.fi/en/research/sysnum/`.

[9] Aalto, A., Alku, P., and Malinen, J. A LF-pulse from a Simple Glottal Flow Model, *MAVEBA2009 Proceedings*, Florence, Italy, 2009.

[10] Aalto, A., Aalto, D., Malinen, J., and Vainio, M. *24th Nordic seminar on computational mechanics Proceedings*. Helsinki, Finland, 2011.

[11] Alku, P. Glottal wave analysis with pitch synchronous iterative adaptive inverse filtering, *Speech Communication*, 11:109–118,1992.

[12] Horáček, J., Šidlof, P., and Švec, J. Numerical simulation of self-oscillations of human vocal folds with Hertz model of impact forces, *J. Fluids and Structures* 20:853–869, 2005.

[13] Morse, P. and Ingard, K. *Theoretical Acoustics*. McGraw Hill, 1968.

[14] Hannukainen, A., Lukkari, T., Malinen, J., and Palo, P. Vowel formants from the wave equation, *J. Acoust Soc. Am.* 122(EL1–EL7), 2007.

[15] Horáček, J. and Švec, J. Aeroelastic model of vocal-fold-shaped vibrating element for studying the phonation threshold, *J. Fluids and Structures* 16:931–955, 2002.

[16] Titze, I. Physiologic and acoustic differences between male and female voices, *J. Acoust. Soc. Am.*, 85(4):1699–1707,1989.

[17] Chhetri, D. K., Zhang, Z., and Neubauer, J. Measurement of Young's modulus of vocal folds by indentation, *Journal of Voice*, 25:1–7, 2011.

[18] Pinheiro, J. C. and Bates, D. M. *Mixed-effects models in S and S-PLUS*, 2000, Springer, New York.

[19] Šidlof, P., Horáček, J., Řidký, V. Parallel CFD simulation of flow in a 3D model of vibrating human vocal folds. *Computers & Fluids*, 2012, Article in press.

[20] Honda, K., Hirai, H, Masaki, S., and Shimada, Y. Role of vertical larynx movement and cervical lordosis in F0 control. *Language and Speech*, 42:4, 401–411, 1999.

[21] Jones, J. A. and Keough, D. Auditory-motor mapping for pitch control in singers and nonsingers. *Exp. Brain Res.*, 190, 279–287, 2008.

[22] Boltežar, I. H., Burger, Z. R., and Z̈argi, M. Instability of voice in adolescence: Pathologic condition or normal developmental variation? *J. Periatrics*, 130:2, 185–190, 1997.